

pathway, the MAPK kinase and MAPK are Pbs2 and Hog1, respectively (18, 19). We found that, like STE11, MEKK1 responds to different stimuli for the selective regulation of at least two MAPK pathways.

Nocodazole treatment of cells did not significantly activate ERK (13). Thus, MEKK1 activation in response to microtubule disruption selectively stimulates JNK. Nocodazole, cold stress, and mild hyperosmolarity all require MEKK1 for JNK activation. The common feature of each of these stresses is a cell shape change, suggesting that MEKK1 activates JNK in response to sensors that detect shape changes. MEKK1^{-/-} cells have a diminished capacity to survive stresses including mild hyperosmolarity and nocodazole-induced disruption of microtubules (Fig. 5). Thus, MEKK1 is required for survival during environmental challenges that stress cells. In normal medium, the growth of MEKK1^{-/-} and wild-type ES cells is similar. Treatment of ES cells with sorbitol inhibited the growth of MEKK1^{-/-} cells relative to wild-type ES cells (Fig. 5A). In addition to sorbitol-induced growth arrest, the number of apoptotic cells was substantially greater for MEKK1^{-/-} compared with wild-type ES cells (Fig. 5B). MEKK1^{-/-} cells were also substantially more sensitive to nocodazole-induced apoptosis (Fig. 5, C and D). MEKK1 expression in transfected MEKK1^{-/-} clones restored the survival response to that of wild-type ES cells just as it reconstituted JNK activation in response to nocodazole treatment.

The antiapoptotic function of MEKK1 activation has been defined by its targeted disruption. The findings define the ability of MEKK1 to enhance the survival of cells after a stress response. MEKK1 promotion of cell survival is opposite to its described proapoptotic function initiated when it is cleaved by caspases (11). Caspase cleavage of MEKK1 releases a 91-kD activated kinase domain that further amplifies caspase activity committing cells to apoptosis; activated full-length 196-kD MEKK1 activates neither caspases nor apoptosis (20). Thus, there is a dual role for MEKK1 controlled by its cleavage. Caspases act as switches to convert the MEKK1 survival signal to a proapoptotic response.

References and Notes

1. M. Russell, C. A. Lange-Carter, G. L. Johnson, *J. Biol. Chem.* **270**, 11757 (1995).
2. G. R. Fanger, N. L. Johnson, G. L. Johnson, *EMBO J.* **16**, 4961 (1997).
3. G. R. Fanger et al., *J. Biol. Chem.* **273**, 3476 (1998).
4. C. A. Lange-Carter, C. M. Pleiman, A. M. Gardner, K. J. Blumer, G. L. Johnson, *Science* **260**, 315 (1993).
5. A. Minden, A. Lin, F. Claret, A. Abo, M. Karin, *Cell* **81**, 1147 (1995).
6. C. Widmann and G. L. Johnson, unpublished data.
7. C. A. Lange-Carter and G. L. Johnson, *Science* **265**, 1458 (1994).
8. G. R. Fanger and G. L. Johnson, unpublished data.
9. N. J. Avdi et al., *J. Biol. Chem.* **271**, 33598 (1996).
10. T. Ishizuka et al., *ibid.*, p. 12762.
11. C. Widmann, P. Gerwins, N. L. Johnson, M. B. Jarpe, G. L. Johnson, *Mol. Cell. Biol.* **18**, 2416 (1998).

12. Genomic DNA clones corresponding to the MEKK1 locus were cloned from a λ FixII phage library prepared from mouse strain 129/sv (Stratagene). The targeting vector was constructed by inserting a 3.8-kb Bam H1–Bam H1 fragment from the 5' end of the genomic clone into the Sal I site of the targeting vector. A 2.0-kb Not I–Sal I fragment from the 3' end of the genomic clone was inserted into the Cla I and Xho I sites of the targeting vector. This construct deleted 132 codons, including the ATG start site in exon 1 of MEKK1, and inserted the neo-resistance gene and polyadenylation signal in the antisense orientation. The linearized construct was introduced into CCE ES cells by electroporation. G418-resistant ES cells were screened for homologous recombination by Southern (DNA) blotting. The frequency of homologous recombination was ~1 in 70. For the generation of MEKK1^{-/-} ES cells, the MEKK1^{+/-} clones were grown at increasing concentrations of G418 up to 10 mg/ml. Two feeder cell-independent CCE MEKK1^{-/-} clones were used for analysis.
13. T. Yujiri, S. Sather, G. R. Fanger, G. L. Johnson, data not shown.
14. JNK activity was assayed by solid-phase kinase assay with GST-c-Jun₁₋₇₉ (GST-Jun) bound to glutathione-Sepharose beads [M. Hibi, A. Lin, T. Smeal, A. Minden, M. Karin, *Genes Dev.* **7**, 2135 (1993)]. The GST-Jun bead assay was verified by JNK immunoprecipitation and in vitro kinase assay with GST-Jun as substrate.
15. MEKK1 was immunoprecipitated from cell lysates with rabbit antiserum to recombinant MEKK1 sequences (17). The immunoprecipitates were used in in vitro kinase assays with kinase-inactive MKK4.
16. I. Sanchez, et al., *Nature* **372**, 794 (1998).
17. ERK 2 was immunoprecipitated from cell lysates with the C-14 antibody (Santa Cruz Biotechnology, Santa Cruz, CA). Myelin basic protein was used as substrate in in vitro kinase assays [S. J. Cook and F. McCormick *Science* **262**, 1069 (1993)]. p38 was immunoprecipitated with a rabbit antiserum to the COOH-terminus of the kinase, and in vitro kinase assays were conducted with recombinant ATF-2 as substrate [P. Gerwins, J. L. Blank, G. L. Johnson, *J. Biol. Chem.* **272**, 8288 (1997)].
18. I. Herskowitz, *Cell* **80**, 187 (1995).
19. F. Posas and H. Saito, *Science* **276**, 1702 (1997).
20. T. Schlesinger and G. L. Johnson, in preparation.
21. We thank S. Webb and G. Keller for help with ES cell culture. Supported by NIH grants DK37871 and GM30324.

1 May 1998; accepted 3 November 1998

Mutation-Specific Functional Impairments in Distinct Tau Isoforms of Hereditary FTDP-17

Ming Hong, Victoria Zhukareva, Vanessa Vogelsberg-Ragaglia, Zbigniew Wszolek, Lee Reed, Bruce I. Miller, Dan H. Geschwind, Thomas D. Bird, Daniel McKeel, Alison Goate, John C. Morris, Kirk C. Wilhelmsen, Gerard D. Schellenberg, John Q. Trojanowski, Virginia M.-Y. Lee*

Tau proteins aggregate as cytoplasmic inclusions in a number of neurodegenerative diseases, including Alzheimer's disease and hereditary frontotemporal dementia and parkinsonism linked to chromosome 17 (FTDP-17). Over 10 exonic and intronic mutations in the *tau* gene have been identified in about 20 FTDP-17 families. Analyses of soluble and insoluble tau proteins from brains of FTDP-17 patients indicated that different pathogenic mutations differentially altered distinct biochemical properties and stoichiometry of brain tau isoforms. Functional assays of recombinant tau proteins with different FTDP-17 missense mutations implicated all but one of these mutations in disease pathogenesis by reducing the ability of tau to bind microtubules and promote microtubule assembly.

FTDP-17 comprises a group of hereditary neurodegenerative syndromes with diverse but overlapping clinical and neuropathologi-

cal features (1, 2). The signature lesions of FTDP-17 brains are insoluble filamentous aggregates of hyperphosphorylated tau proteins

Table 1. Summary of MT binding and MT assembly promoting properties of WT and mutant tau. AU, absorbance unit.

	MT binding		MT assembly promotion		
	B_{max} (μ M) [†]	K_d (μ M) [†]	Lag time (min)	Initiation rate (AU/min)	A_{350} max [†]
WT	1.238 ± 0.042	0.039 ± 0.006	2	0.15	0.533 ± 0.003
N279K	1.265 ± 0.055	0.056 ± 0.012	2	0.16	0.538 ± 0.005
P301L	0.883 ± 0.047**	0.079 ± 0.016*	5	0.14	0.522 ± 0.005
V337M	0.909 ± 0.037**	0.048 ± 0.009	3	0.13	0.482 ± 0.005*
R406W	0.628 ± 0.033**	0.089 ± 0.021*	5	0.04	0.406 ± 0.012**

[†]Mean ± SEM. *P < 0.05, **P < 0.01.

REPORTS

similar to brains of patients with Alzheimer's disease (AD) (3). The absence of senile plaques and Lewy bodies indicates that neuronal loss could be a consequence of the tau pathology. Genetic linkage analysis demonstrated association of the tau gene with FTDP-17 (4-6). Missense mutations in exons 9 [Gly²⁷² to Val (G272V)], 10 [Asn²⁷⁹ to

Lys, Pro³⁰¹ to Leu] (N279K, P301L), 12 [Val³³⁷ to Met] (V337M), and 13 [Arg⁴⁰⁶ to Trp] (R406W) (7) [numbered according to

the longest tau isoform (8)] as well as three intronic mutations close to the 5' splice site of exon 10 have been reported. Here we

M. Hong, V. Zhukareva, V. Volgelsberg-Ragaglia, L. Reed, J. Q. Trojanowski, V.M.-Y. Lee, Center for Neurodegenerative Disease Research, Department of Pathology and Laboratory Medicine, University of Pennsylvania School of Medicine, Philadelphia, PA 19104, USA. Z. Wszolek, Department of Neurology, Mayo Clinic Jacksonville, Jacksonville, FL 32224, USA. B. I. Miller, Department of Neurology, University of California, San Francisco, CA 94143, USA. D. H. Geschwind, Department of Neurology, Program in Neurogenetics, Reed Neurological Research Center, University of California at Los Angeles, Los Angeles, CA 90095, USA. T. D. Bird, Veterans Affairs Puget Sound Health Care System, Seattle Division, and Department of Neurology, University of Washington, Seattle, WA 98195, USA. D. McKeel, Department of Pathology, Washington University School of Medicine, St. Louis, MI 63110, USA. A. Goate, Department of Psychiatry, Washington University School of Medicine, St. Louis, MI 63110, USA. J. C. Morris, Department of Neurology, Washington University School of Medicine, St. Louis, MI 63110, USA. K. C. Wilhelmsen, Department of Neurology, University of California, and Gallo Clinic and Research Center, San Francisco, CA 94110, USA. G. D. Schellenberg, Veterans Affairs Puget Sound Health Care System, Seattle Division, and Department of Neurology, University of Washington, and Department of Pharmacology, Division of Gerontology and Geriatric Medicine, Department of Medicine, University of Washington, Seattle, WA 98195, USA.

*To whom correspondence should be addressed. Email: vmylee@mail.med.upenn.edu

Fig. 2. Biochemical profile of tau in FTDP-17 brains. (A) Insoluble tau in FTDP-17 brains. (A) Insoluble tau in FTDP-17 brains contains either 4Rtau or all six tau isoforms. Sarkosyl-insoluble tau was extracted as described (10) from autopsy-derived frontal gray matter of AD, PPND (N279K), DDPAC (exon 10 splice + 14 mutation), Montreal (P301L), Seattle BK (V337M), or FTD004 (R406W) patients. A portion of each sample was dephosphorylated by incubation with *E. coli* alkaline phosphatase (18). The dephosphorylated and nondephosphorylated samples plus a mixture of six recombinant human brain tau isoforms were resolved on 7.5% SDS polyacrylamide gels and transferred to a nitrocellulose membrane for immunoblot analysis with T14, a phosphorylation-independent monoclonal antibody to tau (17). (B to E) Soluble tau from FTDP brains with different 4R/3R tau ratios. To determine the isoform composition of soluble tau in affected frontal cortex (B and C) and unaffected cerebellum (D and E), the frontal gray or cerebellar white matter was extracted in high-salt RA buffer [0.1 M MES, 0.5 mM MgSO₄, 1 mM EGTA, 2 mM dithiothreitol (pH 6.8), and a mixture of protease inhibitors (2 mM phenylmethylsulfonyl fluoride and *N*-tosyl-L-phenylalanylchloromethyl ketone, *N*-tosyl-L-leucylchloromethyl ketone, leupeptin, pepstatin, and soybean trypsin inhibitor, each at 1 μg/ml)] as described (17). The heat-stable fractions were dephosphorylated with *E. coli* alkaline phosphatase overnight at 37°C (10). The nondephosphorylated (-) and dephosphorylated (+) samples along with a mixture of six isoforms of recombinant tau proteins were resolved on 7.5% SDS-polyacrylamide gel and transferred to nitrocellulose replica for immunoblotting with a rabbit polyclonal antiserum to recombinant tau (17026). ¹²⁵I-labeled protein A was used for immunoblot quantitation (B). After dephosphorylation, each of the biopsy-derived tau isoforms aligned exactly with the corresponding recombinant human brain tau isoform. Quantitative data are shown in (C) where columns represent mean ± SEM values of biopsies (n = 4). The 2N, 1N, and 0N tau isoforms compose 9.5% ± 0.4%, 53.7% ± 0.4%, and 36.8% ± 0.8% of total tau.

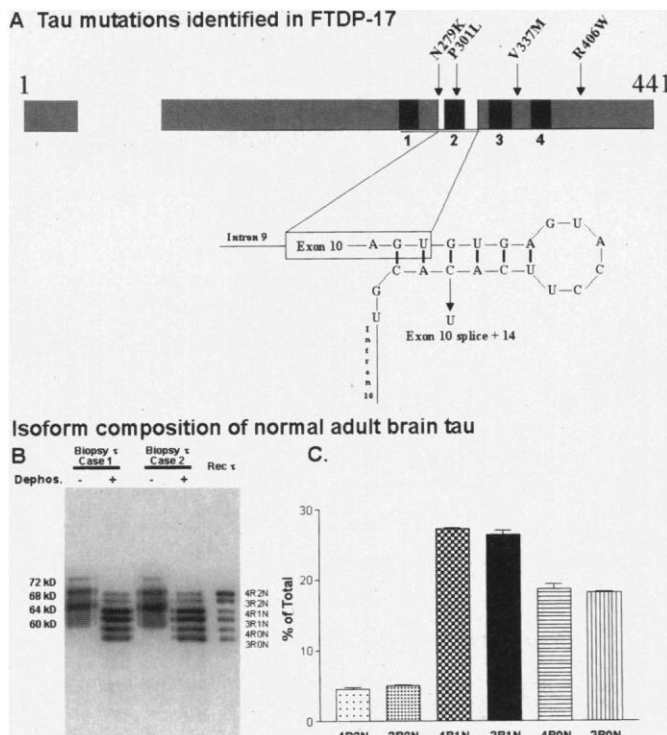
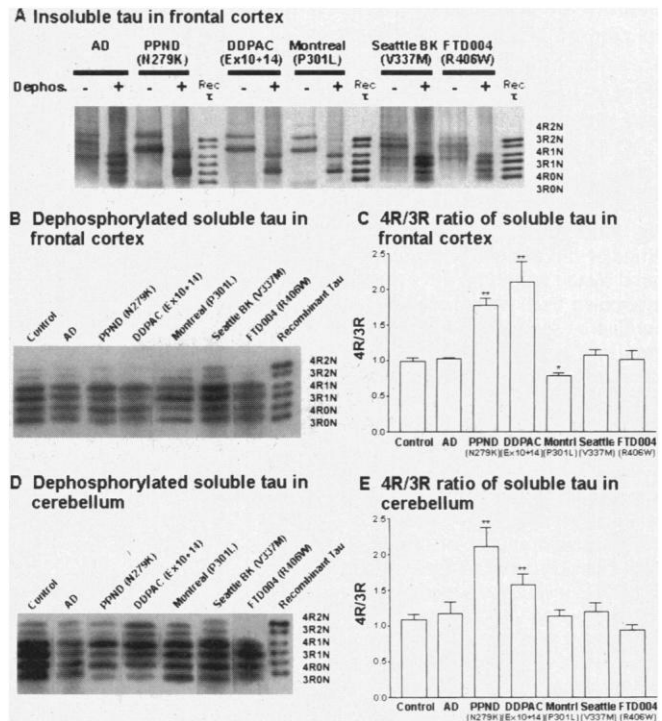


Fig. 1. (A) The tau mutations in FTDP-17 studied here are illustrated on a schematic of the longest central nervous system tau isoform (7). The V337M mutation is located in the interrepeat region between 3 and 4, R406W near the COOH-terminus, and N279K and P301L within exon 10. The proposed RNA stem-loop structure at the exon 10 splice site is also shown. The C-to-U intronic mutation is located within the stem-loop at exon 10 splice site + 14. (B and C) Cortical biopsy samples were immediately extracted in high-salt (0.75 M NaCl) reassembly (RA) buffer [0.1 M MES, 0.5 mM MgSO₄, 1 mM EGTA, 2 mM dithiothreitol (pH 6.8), and a mixture of protease inhibitors (2 mM phenylmethylsulfonyl fluoride and *N*-tosyl-L-phenylalanylchloromethyl ketone, *N*-tosyl-L-leucylchloromethyl ketone, leupeptin, pepstatin, and soybean trypsin inhibitor, each at 1 μg/ml)] as described (17). The heat-stable fractions were dephosphorylated with *E. coli* alkaline phosphatase overnight at 37°C (10). The nondephosphorylated (-) and dephosphorylated (+) samples along with a mixture of six isoforms of recombinant tau proteins were resolved on 7.5% SDS-polyacrylamide gel and transferred to nitrocellulose replica for immunoblotting with a rabbit polyclonal antiserum to recombinant tau (17026). ¹²⁵I-labeled protein A was used for immunoblot quantitation (B). After dephosphorylation, each of the biopsy-derived tau isoforms aligned exactly with the corresponding recombinant human brain tau isoform. Quantitative data are shown in (C) where columns represent mean ± SEM values of biopsies (n = 4). The 2N, 1N, and 0N tau isoforms compose 9.5% ± 0.4%, 53.7% ± 0.4%, and 36.8% ± 0.8% of total tau.

describe how five different FTDP-17 mutations differentially impair specific properties of tau (Fig. 1A).

In the adult human brain, six different tau isoforms are generated by alternative mRNA splicing of 11 exons in the *tau* gene (8, 9). These isoforms differ by the presence or absence of one or two (29 or 58 amino acids long, respectively) NH₂ inserts and by a COOH region with three (3Rtau) or four (4Rtau) imperfect 18-amino acid microtu-

bule (MT)-binding repeats, each of which is separated by an interrepeat domain of 13 or 14 amino acids (8). We first determined the relative abundance of the six tau isoforms in brain by analyzing dephosphorylated tau (10) from biopsy samples of normal human cortex (11) (Fig. 1B). Quantitation of dephosphorylated 3Rtau isoforms with two, one, or no NH₂-terminal inserts and the corresponding 4Rtau isoforms from four different brain biopsies showed that the ratio of 4Rtau to

3Rtau isoforms (4R/3R) was about 1 (Fig. 1C).

Consistent with the findings of Clark *et al.* (6), dephosphorylated insoluble tau from frontal cortex of affected family members with N279K or P301L mutations or with an intronic mutation close to the 5' exon 10 splice site comigrated exclusively with 4Rtau isoforms (Fig. 2A). In contrast, dephosphorylated insoluble tau from affected members of families with a V337M or a R406W mutation comigrated with all six tau isoforms (Fig. 2A). We also compared the 4R/3R tau ratio in the soluble fractions of the same FTDP-17 samples with the ratios observed in similar samples from AD patients and age-matched controls (Fig. 2, B and C). A twofold increase was observed in the disinhibition-dementia-parkinsonism-amyotrophy complex (DDPAC) sample (exon 10 5' splice mutation). A similar twofold increase also was observed in samples from pallido-ponto-nigral degeneration (PPND) subjects with the N279K mutation. In sharp contrast, the brain from an affected member of the Montreal kindred with the exon 10 P301L mutation showed a 25% reduction in 4R/3R of soluble tau that may reflect the selective incorporation of 4Rtau isoforms into insoluble aggregates. These data suggest that the N279K and P301L mutations result in selective aggregation of 4Rtau into insoluble filamentous lesions by different mechanisms and that the N279K mutation may increase 4R/3R by enhanced splicing of exon 10.

Fig. 3. Microtubule-binding properties of tau are differentially altered by tau mutations. MTs were assembled from phosphocellulose purified bovine tubulin (Cytoskeleton, Inc.) as described (17). Taxol-stabilized MT dimer (3 μM) was incubated with 0 to 2 μM recombinant tau at 37°C for 20 min. A sucrose cushion was underlaid and the bound and free tau were separated by centrifugation (50,000g) at 25°C for 20 min. ¹²⁵I-labeled quantitative immunoblot analysis with the polyclonal antiserum to tau (17026) was performed to determine bound and free tau. Each experiment was repeated at least three times with at least two recombinant tau preparations. Binding curves were generated by plotting bound versus free tau and fitting data by nonlinear regression with the standard binding equation (bound tau) = $B_{max} \times (\text{free tau}) / [K_d + (\text{free tau})]$.

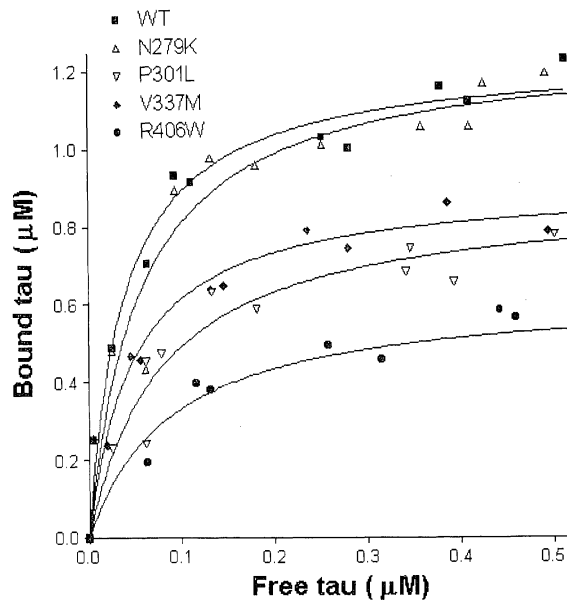
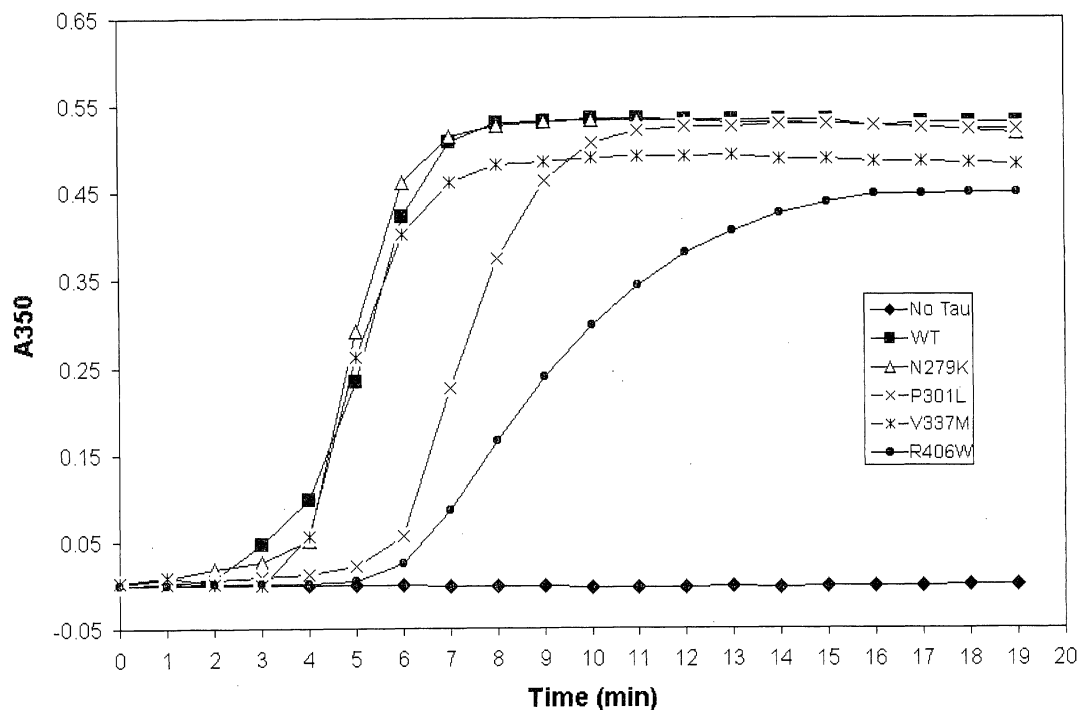


Fig. 4. Missense mutations reduce the ability of tau to promote MT assembly. To assess the abilities of WT and mutant tau proteins to promote MT assembly, light-scattering assays were performed (13, 14) with some modifications. Briefly, 35 μM bovine tubulin monomer was mixed at 4°C with 15 μM WT or mutant tau in RA buffer supplemented with 1 mM guanosine triphosphate. Turbidity was measured in quartz cuvettes by reading the absorbance at 350 nm (A_{350}) with a Beckman DU640 spectrophotometer. Samples were gradually warmed to 37°C with a defined rate and turbidity continuously measured at 1-min intervals. Duplicate samples were examined in each experiment and each experiment was repeated at least three times with at least two different recombinant tau preparations. A representative assay result is shown. In the absence of tau, turbidity remains at baseline, indicating minimal MT assembly. In the presence of WT tau, turbidity increased at an initiation rate of 0.15 absorbance unit per minute



after a lag time of about 2 min, and plateaus within about 7 min when maximal MT assembly is reached.

Because the cerebellum is nearly devoid of tau pathology in FTDP-17 patients (3), 4R/3R in soluble fractions of cerebellum should not be perturbed by an insoluble pool of aggregated tau. The finding of a 1.5- to 2-fold increase in 4R/3R in the PPN and DDPAC cerebellum but a 4R/3R of about 1 in the Montreal cerebellum (Fig. 2, D and E) is consistent with the idea that the N279K but not the P301L mutation increases splicing of exon 10. Analysis of affected brains from both Seattle BK (V337M) and FTD004 (R406W) kindreds showed no change in the 4R/3R ratio compared with the ratios in the soluble frontal cortex and cerebellum fractions of AD patients and controls.

To determine how different mutations in the tau gene alter specific tau functions, we compared the MT-binding properties of wild type (WT) and mutant recombinant tau proteins (12) with a fixed amount of taxol-stabilized MTs by measuring the amounts of bound and unbound tau (Fig. 3). Both WT and N279K mutant tau proteins bound equally well to MTs, with maximum binding (B_{max}) of about 1.2 μ M, whereas P301L, V337M, and R406W mutant tau proteins exhibited much lower B_{max} values of 0.88, 0.91, and 0.63 μ M, respectively (Fig. 3 and Table 1). Surprisingly, the tau isoform with the R406W mutation had the lowest MT-binding capacity (about half that of WT tau) despite the fact that it is not near the MT binding domains. None of the mutant tau proteins was able to bind MTs as avidly as WT tau (Fig. 3 and Table 1), and the affinity of the R406W tau mutant was the lowest. Thus, our data suggest that one of the dysfunctional consequences of the FTDP-17 missense mutations (except for N279K) in tau is a reduction in their binding capacity as well as their binding affinity for MTs.

We next assessed the ability of WT and mutant tau proteins to promote MT assembly by the light-scattering technique (13, 14). This assay (Table 1) measures the lag time required to nucleate MTs, the ability of tau to initiate MT assembly, and the maximum amount of MT polymers that form in the presence of tau. The N279K mutation did not affect the ability of tau to promote MT assembly. However, P301L, R406W, and V337M mutant tau proteins nucleated MTs less efficiently than WT tau. The R406W tau mutant had the slowest initiation rate of MT assembly followed by P301L and V337M tau mutants (Fig. 4 and Table 1). The R406W tau mutant was the most defective in promoting MT assembly because the maximum polymer mass formed in the presence of this mutant was only about 75% that formed by WT tau. Despite a longer lag time for MT nucleation, the P301L tau mutant promoted MT assembly to the same extent as WT tau and N279K tau mutants.

This study demonstrates that some FTDP-17 mutations alter the MT-binding properties of tau, and others alter the ratio of 4R/3R tau isoforms. Intronic mutations (for example, in the DDPAC kindred) presumably alter 4R/3R tau ratios by weakening a stem-loop structure at the 5' splice site of exon 10, which normally inhibits the inclusion of exon 10 into tau mRNA (5). How the N279K mutation increases 4Rtau production is less clear. Because the N279K mutation does not alter the binding of tau to MTs or decrease the ability of tau to promote MT assembly, the selective aggregation of 4Rtau into filamentous lesions probably results from overproduction of 4Rtau proteins by increasing the inclusion of exon 10 into more tau mRNAs. Presumably, this mutation could act by altering an exon-splicing enhancer (ESE) sequence in exon 10 (15). At the nucleotide level, the N279K mutation changes the normal sequence of TAAGAA to GAAGAA, a potential GAR (where R is a purine) ESE motif (6). These ESE sequences have been shown to bind to the SR family of proteins (16), which are essential factors for splice site selection in the alternative splicing of cellular and viral mRNAs.

In contrast, the missense mutations P301L, V337M, and R406W alter the biochemical properties of tau. The P301L mutation in exon 10 reduces the MT-binding affinity of 4Rtau and diminishes the number of 4Rtau proteins that could bind to MTs. As P301 is part of a highly evolutionarily conserved PGGG motif in all MT-binding repeats and is located in the MT-binding repeat specific for 4Rtau, it is not surprising that this missense mutation affects only 4Rtau. Similarly, the V337M mutation also interfered with the interaction of tau with MTs, but all six tau isoforms were affected because the V337M mutation is located in exon 12, which is included in all tau splice variants. Finally, despite the fact that R406W is not located in or near a MT-binding repeat, it had the most profound effects on the ability of tau to interact with MTs, and it is possible that a R to W substitution alters the conformation of tau, thereby reducing its binding to MTs, as is thought to occur after phosphorylation at Ser³⁹⁶ and Ser⁴⁰⁴ (17). The P301L, V337M, and R406W missense mutations may cause FTDP-17 by a partial loss of function mechanism. A slight decrease in the binding of mutant tau to MTs could destabilize MTs over time and have deleterious effects, including a disruption of axonal transport. However, these mutations also could result in a toxic gain of function because reduced binding of mutant tau leads to increased free cytoplasmic tau and an increased propensity to form insoluble aggregates. Similarly, the overproduction of 4Rtau due to an intronic

mutation close to the exon 10 5' splice site and to the N279K mutation also could result in a partial loss of function and a toxic gain of function. There are no data currently on the toxicity of 4R versus 3R tau protein in vitro. Indeed, tauopathies containing either 4R aggregates (some of the FTDP-17 kindreds described here), 3R aggregates (as observed in Pick's disease), or both 4R and 3R aggregates (as in AD and other FTDP-17) demonstrate that aggregation of both or either variety can cause disease.

References and Notes

1. N. L. Foster et al., *Ann. Neurol.* **41**, 706 (1997).
2. K. C. Wilhelmsen, T. Lynch, T. G. Nygaard, *Am. J. Hum. Genet.* **55**, 1159 (1994).
3. M. G. Spillantini, T. D. Bird, B. Ghetti, *Brain Pathol.* **8**, 387 (1998); L. A. Reed et al., *J. Neuropathol. Exp. Neurol.* **57**, 588 (1998).
4. P. Poorkaj et al., *Ann. Neurol.* **43**, 815 (1998); M. G. Spillantini et al., *Proc. Natl. Acad. Sci. U.S.A.* **95**, 7737 (1998).
5. M. Hutton et al., *Nature* **393**, 702 (1998).
6. L. N. Clark et al., *Proc. Natl. Acad. Sci. U.S.A.* **95**, 13103 (1998).
7. Amino acids are designated by the single-letter code as follows: A, Ala; C, Cys; D, Asp; E, Glu; F, Phe; G, Gly; H, His; I, Ile; K, Lys; L, Leu; M, Met; N, Asn; P, Pro; Q, Gln; R, Arg; S, Ser; T, Thr; V, Val; W, Trp; Y, Tyr.
8. M. Goedert, M. G. Spillantini, R. J. Jakes, D. Rutherford, R. A. Crowther, *Neuron* **3**, 519 (1989).
9. A. Andreadis, M. W. Brown, K. S. Kosik, *Biochemistry* **31**, 10626 (1992).
10. V. M.-Y. Lee, B. J. Balin, L. Otvos Jr., J. Q. Trojanowski, *Science* **251**, 675 (1991).
11. E. S. Matsuo et al., *Neuron* **13**, 989 (1994).
12. Site-directed mutagenesis was used to introduce a series of missense mutations into pRK172/T40, a prokaryotic expression vector carrying the cDNA of the longest human central nervous system brain tau isoform (8). WT and mutant recombinant tau proteins were produced in an isopropyl β -D-thiogalactopyranoside-treated BL21 *Escherichia coli* strain and purified by Mono-S FPLC (13). The purified WT and mutant recombinant tau proteins were assessed by Coomassie blue-stained SDS-polyacrylamide gel electrophoresis. The concentrations of WT and mutant recombinant tau proteins were determined with BCA reagents (Pierce), densitometric scanning of Coomassie blue-stained gels, and quantitative immunoblotting with ¹²⁵I-labeled protein A as a secondary antibody.
13. N. Gustke, B. Trinczek, J. Biernat, E.-M. Mandelkow, E. Mandelkow, *Biochemistry* **33**, 9511 (1994).
14. F. Gaskin, C. R. Cantor, M. L. Shelanski, *J. Mol. Biol.* **89**, 737, (1974).
15. R. Xu, J. Teng, T. A. Cooper, *Mol. Cell Biol.* **13**, 3660 (1993); A. Watakabe, K. Tanaka, Y. Shimura, *Genes Dev.* **7**, 407 (1993); A. Lavignier, H. La Branche, A. R. Kornblihtt, B. Chabot, *Science* **260**, 219 (1993).
16. X. D. Fu, *Nature* **365**, 82 (1993); A. M. Zahler, K. M. Neugebauer, W. S. Lane, M. B. Roth, *Science* **260**, 219 (1993).
17. G. T. Bramblett et al., *Neuron* **10**, 1089 (1993).
18. M. Goedert, M. G. Spillantini, N. J. Cairns, R. A. Crowther, *ibid.* **8**, 159 (1992).
19. Supported by grants from the National Institute on Aging. We thank E. Holzbaue for critically reading the manuscript; J. J. Kulstad, C. Li, and R. Dhupar for technical assistance; M. Goedert for human recombinant tau proteins; our colleagues in the Departments of Neurology, Pathology and Laboratory Medicine, and Psychiatry for their support; and the families of the patients who made this research possible.

15 September 1998; accepted 3 November 1998